ADVANCED ELECTRONIC MATERIALS Open Access
www.advelectronicmat.de

Bioinspired PVDF Piezoelectric Generator for Harvesting Multi-Frequency Sound Energy

Bangyan Duan, Kefan Wu, Xiaoyang Chen, Jinyan Ni, Xin Ma, Weishuai Meng, Kwok-ho Lam,* and Ping Yu**

With the rapid development of micro-energy harvesting technology, noise has great potential as a new type of micro-energy source by developing a high-performance acoustic energy harvester (AEH). Nevertheless, the challenges of harvesting energy from noise are low acoustic energy density, multi-frequency mixed sound, and unstable sound pressure. Piezoelectric-based AEHs are proposed as a solution, but most reported devices need to work at a certain frequency and very high sound pressure, and exhibit the disadvantages of being bulky and heavy when using an extra sound-pressure amplifier. Here, the eardrum and cochlea bioinspired polyvinylidene fluoride (PVDF) piezoelectric generator which is lightweight, compact, has a simple structure and is low-cost, harvests multi-frequency sound energy. Although using the commercial pure PVDF membrane, the prepared AEH still presents a high acoustoelectric conversion performance with an output power of 8.45 μW and an acoustic sensitivity of 1 V Pa^{-1} at 200 Hz and 100 dB without using any sound-pressure amplifier through optimizing the structure–vibration–frequency relationship. More importantly, the bioinspired AEHs do not only exhibit the ability of acoustic energy harvesting function but also have the abilities of frequency recognition and acoustic sensing, which show great potential in the application of self-powered acoustic sensors.

1. Introduction

Nowadays, micro-energy harvesting technology has been one of the very important branches of energy technology.[1–3] Different from the conventional large-scale and high-power generation technology, the micro-energy harvesting technique generally has no special requirement for installation and use such as sites, equipment, weather, etc, and mainly focuses on the micro-energy sources around our life and environment.[4,5] The main features of these micro-energy harvesters are compact, portable/wearable, and easy to implement with good environmental adaptability. Among the micro-energy sources, noise is a mechanical wave that propagates in the air and carries mechanical vibration energy.[6] Common noise sources include airplanes, vehicles, high-speed trains, factories, loudspeakers, machines, and expressways, which almost cover all aspects of our life and environment.[7] Noise has become a serious social problem, which is considered as pollution to imperil people's health, for instance, causing irreparable damage to hearing, cardiovascular and neuroendocrine systems especially when the noise level is above 90 dB.[8] Nevertheless, on the other hand, noise is a long-neglected, growing, widespread, and ubiquitous micro-energy source.[9] Therefore, exploring how to make use of the noise would not only identify alternate micro-energy sources but also help reduce noise pollution. More importantly, the lower electrical-power consumption of modern electronic components and the rapid development of wireless portable charging technology opens up unprecedented opportunities and great possibilities for developing noise-based micro-energy harvesting technology.[10]

The most ubiquitous noise is primarily low-frequency (<500 Hz) and high-pressure acoustic waves (>80 dB).[11] As the noise is a multi-frequency acoustic wave while the acoustic pressure is often changed rapidly, its energy input is inefficient, unstable, and intermittent.[12] To harvest this long-neglected energy, a high-performance acoustic energy harvester (AEH) with a high acoustoelectric conversion capability at low frequency and low sound pressure level (SPL) and a wide bandwidth in the noise frequency range is desired.

The state-of-the-art AEHs can be classified into three types based on the working principle: piezoelectric generator,

B. Duan, K. Wu, X. Chen, J. Ni, X. Ma, W. Meng, P. Yu
College of Material Science and Engineering
Sichuan University
Chengdu 610064, P. R. China
E-mail: xiaoyang189@scu.edu.cn; pingyu@scu.edu.cn
K.-ho Lam
James Watt School of Engineering
University of Glasgow
Glasgow, Scotland G12 8QQ, UK
E-mail: kwokho.lam@glasgow.ac.uk
The ORCID identification number(s) for the author(s) of this article can be found under https://doi.org/10.1002/aelm.202300348

DOI: 10.1002/aelm.202300348

triboelectric nanogenerator (TENG), and electromagnetic generator (EMG).[13,14] Due to the low acoustic energy density and the rapid change in sound pressure, the EMG cannot work effectively by using the conductor to cut the magnetic field lines.[15] TENG could produce remarkable electrical output by coupling the triboelectric effect with the electrostatic induction. However, due to the nature of the electrostatic phenomenon, the electrostatic charges can be severely affected by humidity and temperature. Moreover, triboelectric devices generally work through a cycled process of contact and separation between two different materials in the triboelectric series. Thus, the operation of triboelectric devices usually requires precise distance control between the triboelectric components that largely increases the fabrication difficulty and cost of AEHs and the risk of device damage under harsh vibrations and shocks.[16] So far, the most reported AEHs are based on piezoelectricity due to the merits of high sensitivity to slight disturbances, simple structure (capacitor structure), easy fabrication, low fabrication cost, and high environmental stability. Piezoelectric generator generally works through the intrinsic piezoelectric effect of piezoelectric materials to generate charges due to the mechanical deformation of oriented molecular dipoles.[17] As the acoustic energy density of sound is small, the resonant working mode is required to generate as much electrical output as possible in the piezoelectric-based AEHs.[18] However, the major challenge of the piezoelectric generator is the narrow frequency bandwidth. Once the frequency of an acoustic wave is different from the designated resonant frequency of AEH, the performance of the generator would degrade significantly.

In the reported research work on piezoelectric generator-based AEHs, most research focus on improving the electrical outputs by amplifying the incident sound pressure which is one of the effective methods. For example, Bin et al. employed multiple PVDF beam arrays in a quarter-wavelength acoustic resonator to harvest the low-frequency acoustic energy.[19] With the incident sound pressure level (SPL) of 110 dB at 146 Hz, the response voltage of 1.48 V corresponding to the volume power density of 0.002 μW cm^{-3} was measured. By adopting this method, rigid piezoelectric materials, like the lead zirconate titanate (PZT) ceramics, could vibrate at low frequency as the piezoelectric element in the AEH. There are three categories of sound pressure amplification: Helmholtz resonator, half-wave/quarter-wave tube resonator, and acoustic metamaterial.[20] Yang et al. utilized a compliant-top-plate Helmholtz resonator and dual PZT cantilever beams to obtain a stronger vibration of beams for achieving high acoustoelectric conversion through a strong multimode coupling between the resonator and PZT beams.[21] Consequently, the AEH exhibited the output power of 0.137–1.430 mW (0.035–0.36 μW cm^{-3}) at 170–206 Hz and 100 dB SPL. Li et al. placed multiple PZT piezoelectric cantilever plates into a quarter-wavelength tube resonator to obtain a low-frequency AEH.[22] The results showed that the maximum total output voltage harvested was 5.089 V (1.367 μW cm^{-3}) at 199 Hz and 100 dB SPL. Yuan et al. utilized a PZT patch and a metallic substrate with proof mass to form a local resonant acoustic metamaterial to convert the incident sound energy to electrical energy.[23] It demonstrated that an electrical power of 210 μW (0.011 μW cm^{-3}) was harvested at 114 dB SPL and 155 Hz. As seen from the reported work, although Helmholtz or tube resonator could largely amplify the SPL of the incident sound in the resonator, there were still disadvantages of heavy weight, big volume, complicated device structure, and fabrication process. Besides, the piezoelectric-type AEHs with high power still work under a certain resonant frequency and very high SPL, which is more suitable for use in high SPL, single, and specific-frequency sound sources. Therefore, for a high-efficiency acoustoelectric conversion in the actual noise environment, harvesting muti-frequency acoustic energy under the lowest possible SPL is an important development direction for the piezoelectric generator-based AEHs.

Compared with rigid piezoelectric ceramics, the piezoelectric polymer presents the merits of lightweight, flexible, low acoustic velocity, easy fabrication, and processing (cutting to shape or size), which is more easy to realize the vibration or deformation under such a low-frequency acoustic wave,[24] and greater potential for the large-scale implementation in the actual environment. However, due to the low electromechanical coupling factor, it is difficult to employ the piezoelectric polymer directly for the application of high-power AEH. Recently, the synthesis of piezoelectric organic polymer into nanofibers could increase the electrical outputs. Mahanty et al. used poly(vinylidene fluoride)-Mg (PVDF-Mg) nanofibers as an active layer to convert acoustic energy into electrical power with the highest power density of 8.36 μW (0.28 μW cm^{-2}) at an open-circuit resonant frequency of 126 Hz and 120 dB SPL.[25] Two-dimensional MOF modulated PVDF nanofiber was prepared to fabricate a flexible and sensitive nanogenerator based on the piezoelectric composite, exhibiting an improved power density and acoustic sensitivity of 6.25 μW (1.04 μW cm^{-2}) and 0.95 V Pa^{-1} at the incident SPL of 110 dB and 120 Hz, respectively.[26] Hao Shao et al. reported a very high power of 210.3 μW (17.53 μW cm^{-2}) at 230 Hz and 117 dB using polyacrylonitrile (PAN) nanofibers.[27] Most piezoelectric organic polymer nanofibers-based acoustic AEHs are not resonant systems, in which the high acoustoelectric conversion efficiency mainly comes from these slender nanofibers that easily vibrate or deform under a certain level of sound pressure. It was also noticed that such a high power was measured at a very low frequency, and generally decreased quickly with increasing frequency. Although the power of most piezoelectric polymer nanofiber-based AEHs still cannot be comparable to the piezoelectric AEHs using the resonator and PZT ceramics, the piezoelectric polymer nanofiber-based AEHs exhibit the merits of lower-volume, lightweight, and simpler device structure and fabrication process. In the reported work of piezoelectric polymer-based AEHs, much effort was made to improve the piezoelectric performance of the polymer with less attention on the device structure and corresponding vibration mode. To our knowledge, a proper structural design could significantly help to further promote the acoustoelectric conversion performance of AEHs. PVDF and its copolymers are suitable candidates due to their excellent chemical stability, flexibility, lightweight, bio-compatibility, and environmental compatibility.[28,29]

In this work, the human eardrum and cochlea bioinspired structural design was utilized to realize the high acoustoelectric conversion and harvest the multi-frequency sound energy at 100 dB by creating more independent resonant frequencies in a narrow frequency range. Commercial PVDF membrane was chosen and fabricated as the piezoelectric elements. The prepared AEHs are characteristic in muti-frequency acoustic energy

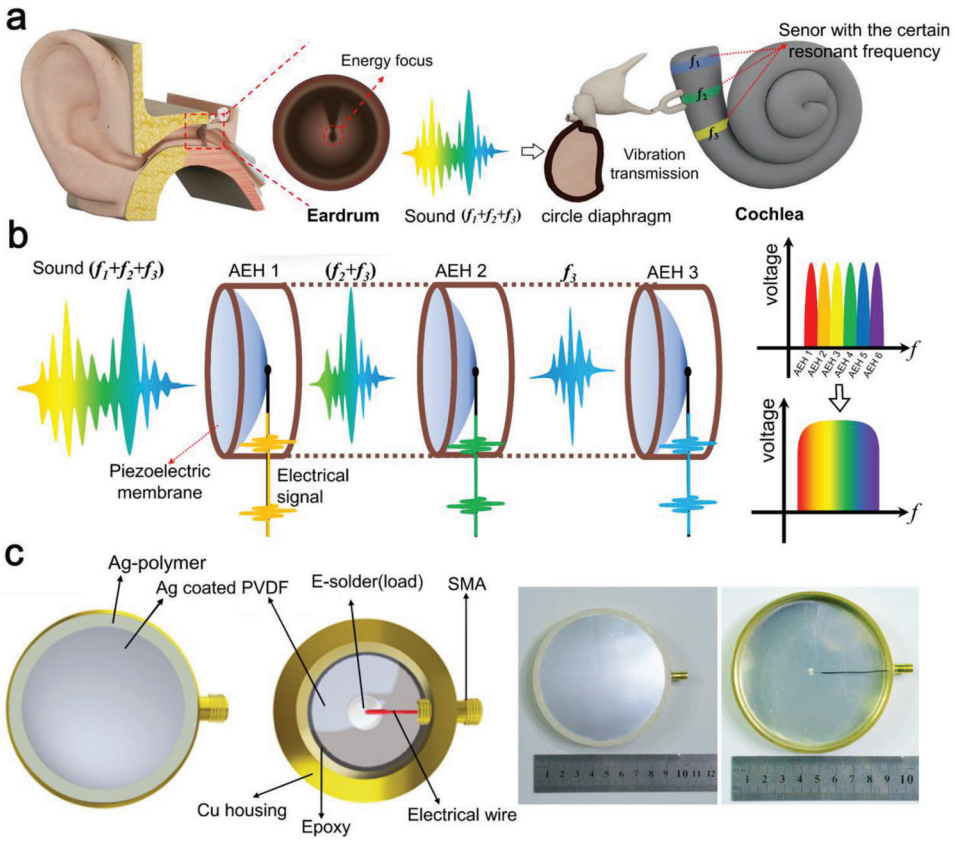

Figure 1. Structure and working principle of the human eardrum and cochlea bioinspired AEHs. a) The structure of the human eardrum and cochlea, as well as the working mechanism of collecting multi-frequency sound by the ear; b) the biomimetic piezoelectric type AEHs with different resonant frequencies in series to harvest the multi-frequency acoustic energy; c) the device structure and the photo of an eardrum bioinspired AEH.

harvesting and no sound-pressure amplifier or extra resonator needed, as well as high acoustoelectric conversion and high acoustic sensitivity. The vibration mode of this AEH was simulated. The effect of structure parameters on the acoustoelectric conversion performance was fully investigated.

2. Results

2.1. Biomimetic Piezoelectric Type AEHs

In this work, the resonant mode is required to improve the electrical outputs by making the resonant frequency of the PVDF element consistent with the frequency of the received sound wave. To maximize the acoustoelectric conversion and solve the narrow frequency bandwidth, a much more effective vibration mode and structural design are desired. The human eardrum and cochlea give inspiration, as shown in **Figure 1**. The human eardrum has a thickness of ≈100 μm, but can effectively collect sound waves even with weak vibration in a wide frequency range of 20–20 000 Hz. The human eardrum is a circular diaphragm with the load on the back side of the center of the membrane.[30] The mechanical energy of the vibration was then further focused and transmitted to the cochlea through the ossicular chain. The cochlea can be treated as acoustic sensors with different resonant frequencies corresponding to be sensitive to vibrations at certain frequencies, and these sensors are connected in series in the cochlea.[31,32] Consequently, the vibration with a certain frequency would transmit along the cochlea until reaching its corresponding resonant region. The structure and working principle of the human eardrum and cochlea could be used to design the piezoelectric type AEHs for harvesting multi-frequency sound waves. Figure 1b shows the proposed biomimetic piezoelectric type AEHs. In this design, a single AEH with a certain resonant frequency is fabricated by a circular diaphragm structure with the load in the center of the backside. By arranging the AEHs with various resonant frequencies in series, the multi-frequency sound waves could be effectively and selectively absorbed through the resonant and non-resonant working mode of the AEH. Since the PVDF membrane has a very low acoustic impedance, the incident sound can pass through the AEH with low attenuation when the sound frequency is inconsistent with the resonance frequency of the AEH. With multiple AEHs of different resonant frequencies, the multi-frequency sound wave could be fully absorbed, which each AEH could realize an acoustoelectric energy conversion efficiency as high as possible by optimizing the vibration at the resonant frequency. Consequently, a high-performance piezoelectric type AEH for the multi-frequency sound could be realized. Figure 1c shows the device structure and the optical image of the eardrum bioinspired AEH.

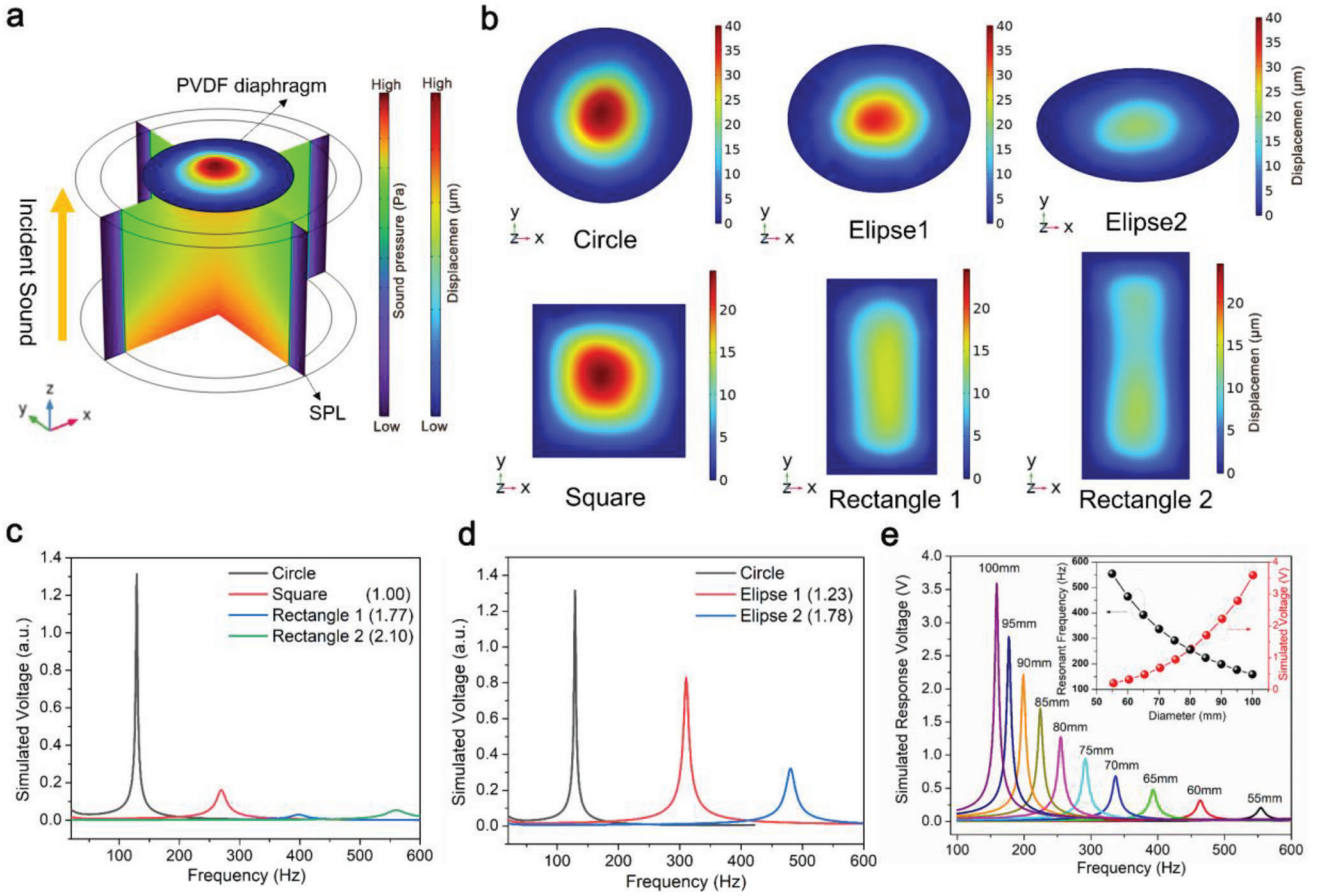

Figure 2. a) Simulated model of a PVDF diaphragm vibrated under the sound; b) the displacement of the PVDF diaphragm with different geometries but identical area at the fundamental resonant frequency under the same SPL; c) the simulated response voltage of circular and rectangular diaphragms with different length-width ratios as a function of frequency; d) the simulated response voltage of circular and elliptical diaphragms with different long axis-short axis ratios as a function of frequency; e) the frequency dependence of simulated response voltage of circular diaphragms as a function of diameter, and the diameter dependences of the fundamental resonant frequency and simulated response voltage (inset).

2.2. Vibration Mode of AEH

To understand the relationship between the geometrical structure and vibration modes of the PVDF diaphragm, the displacement and response voltage of the PVDF diaphragm with different structures are simulated. The simulated mode is constructed as shown in **Figure 2**a (see the supporting information for more details). The PVDF diaphragm vibrates under different single-frequency sounds with an SPL of 100 dB (2 Pa). According to the sweep frequency tests, the resonant frequency, displacement, and response voltage are obtained. As the maximum response voltage generally is obtained at the fundamental frequency, the fundamental frequency vibration mode is the major concern in this work. As shown in Figure 2b, although all the PVDF diaphragms have an identical area, the displacement of the PVDF diaphragm could reach the maximum at the fundamental frequency when adapting a circular geometrical structure. Moreover, the geometry and size of the deformation or vibration region are strongly influenced by the structure of diaphragms. Therefore, the geometrical structure has a significant effect on the resonant frequency, response voltage, and bandwidth.

Compared with the rectangular (Figure 2c) and elliptical (Figure 2d) diaphragms, the circular PVDF diaphragm exhibits the lowest resonant frequency and highest response voltage. The resonance frequency increases with the length-width ratio in the rectangular diaphragms and the ratio of long-axis to short-axis in the elliptical diaphragms. Moreover, the bandwidth obviously increases when the geometry is changed from circle to square and rectangle (Figure 2c) as well as circle to ellipse (Figure 2d). The difference in the geometric structure can be described by the shape asymmetry. The higher shape asymmetry would lead to the formation of a more irregular and unsymmetrical vibration region, in which extra vibrations near the resonant frequency are generated, leading to the enhancement of bandwidth. Since the extra vibrations would disperse the total input mechanical energy, the maximum displacement of the diaphragms and the response voltage at the resonant frequency decrease. Therefore, among the geometries, the circular diaphragm would have the highest response voltage, the lowest resonant frequency, and the narrowest bandwidth due to its highest symmetry. Besides the geometry, the circular diaphragm with different diameters is simulated as shown in Figure 2e. Due to the enlarged vibration

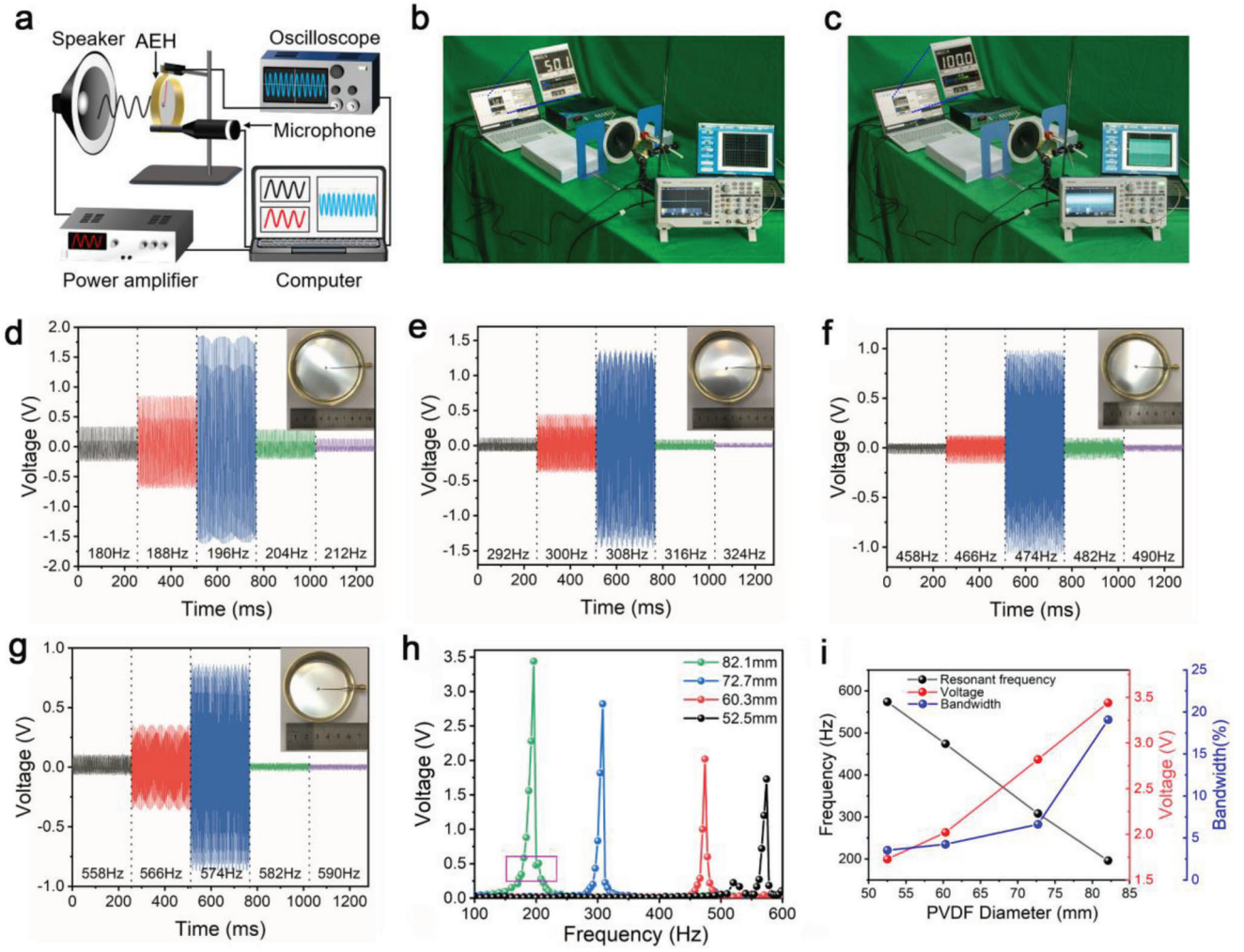

Figure 3. a) Schematic illustration of a testing platform setup; photo of the testing platform b) before opening the loudspeaker and c) opening the loudspeaker; the laptop on the left presents the real-time SPL measured by the microphone, while the laptop on the right shows the electrical signals from the AEH fixed with a distance of 10 cm from the loudspeaker; d–g) the results of acoustoelectric conversion by the AEHs with the diameters of d) 82.1 mm, e) 72.7 mm, f) 60.3 mm, and 52.5 mm at their respective resonant frequencies under a SPL of 100 dB; h) the frequency-dependent response-voltage of four AEHs at 100–600 Hz through the frequency sweep test; i) the resonant frequency, response voltage and the corresponding bandwidth at −10 dB (10%) of AEHs as a function of the PVDF membrane diameter.

region and better flexibility, the resonant frequency drops while the response voltage increases along with the increasing diameter of the circular diaphragm. It is envisaged that the frequency dependence of vibration mode and acoustoelectric conversion performance could be effectively modulated by modifying the geometric structure of the PVDF diaphragm.

2.3. Structural Parameters of AEH

In the design of the eardrum-inspired AEH, the diameter of the PVDF membrane and the backload are two critical parameters that determine the acoustoelectric conversion performance, which are investigated by an open testing platform as shown in **Figure 3**a–c. The platform is built to mimic the practical environment. Initially, the SPL of the quiet environment is about 50.1 dB when the loudspeaker is off, and the electrical signal measured by the oscilloscope is very weak. After turning on the loudspeaker, the SPL of the incident sound near the AEH is kept precisely at 100 dB, while obvious electrical signals can be seen from the oscilloscope, indicating a high electrical output from the AEH. Firstly, the effect of the PVDF membrane diameter (82.1, 72.7, 60.3, and 52.5 mm) on the acoustoelectric conversion performance is investigated. Figure 3d–g exhibits the results of the acoustoelectric conversion of four AEHs with different PVDF membrane diameters at frequencies near their resonant frequencies with the SPL excitation of 100 dB. It can be seen that the 82.1 mm-diameter AEH has the highest peak-to-peak voltage of 3.44 V and the lowest resonant frequency of 196 Hz, while the 52.5 mm-diameter AEH has the lowest peak-to-peak voltage (1.73 V) and the highest resonant frequency (574 Hz). Figure 3h exhibits the response voltage as a function of the frequency of four AEHs in the frequency range of 100–600 Hz. A very high and sharp voltage-response peak is shown in the wide frequency

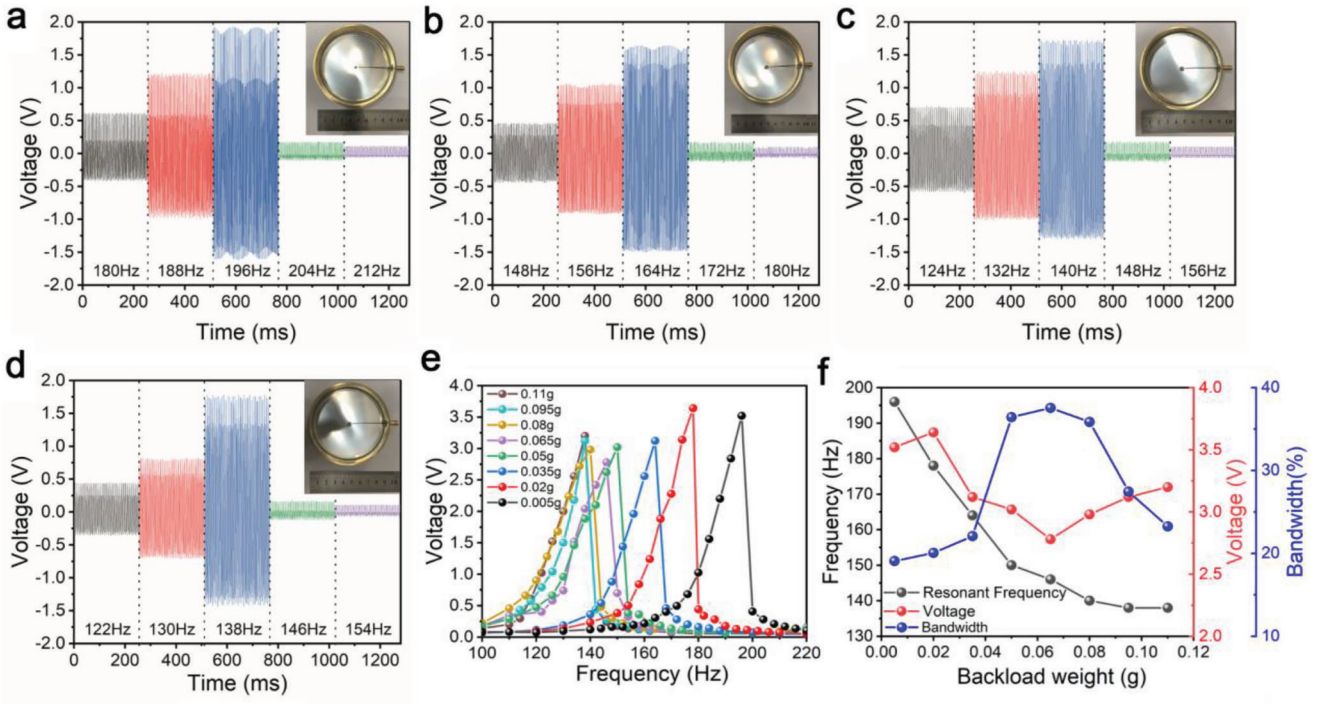

Figure 4. The results of acoustoelectric conversion of AEHs with back loads of a) 0.005 g, b) 0.035 g, c) 0.080 g, and d) 0.095 g at their respective resonant frequencies under an SPL of 100 dB; e) the frequency-dependent response voltage of AEHs with different load weights at 100–220 Hz; h) the resonant frequency, response voltage and the bandwidth at -10 dB of AEH as a function of backload weight.

range without any spurious peak in the AEH samples with diameters of 82.1, 72.7, and 60.3 mm, respectively, which indicates a very clear and single-vibration mode. This also can explain why relatively high response-voltage outputs can be realized in these devices. As shown in Figure 3i, the resonant frequency almost increases linearly with the reducing membrane diameter and could be effectively adjusted in the low-frequency range. Besides, as the diameter of the PVDF membrane is proportional to the effective area for absorbing acoustic energy, the smaller membrane would offer a lower response voltage. The measured results are almost in accord with the above-simulated results. Besides, the bandwidth at -10 dB increases slowly for the AEHs with diameters from 52.5 to 72.7 mm, while the 82.1 mm-diameter AEH shows the highest bandwidth of 17.2% among the devices. The improved bandwidth mainly comes from the contribution of the increased weak electrical output (highlighted as a purple rectangle in Figure 3h).

Besides the diameter of the PVDF membrane, the effect of backload is investigated. **Figure 4**a–d shows that the resonant frequency decreased as a function of the load. The results of the acoustoelectric conversion of AEHs with other load weights are shown in Supporting Information (Figure S1, Supporting Information). Figure 4e exhibits the frequency sweep test results of AEHs with different weights in the frequency range of 100–220 Hz, showing that the load weight can decrease the resonant frequency until reaching 0.08 g. Figure 4i shows the resonant frequency, response voltage, and bandwidth of AEHs as a function of the load. Compared to the diameter of the PVDF membrane, it is more suitable to use the load to fine-tune the resonant frequency within 50 Hz. Besides, the appropriate small increment of load weight (0.005 g → 0.020 g) can improve the response voltage and bandwidth. Further improving the load weight would cause a reduction in the response voltage. When the load weight is further increased, the variations of frequency-dependent bandwidth and response voltage are opposite. When the load weight is increased from 0.02 to 0.05 g, the bandwidth improves from 20.0% to 36.4% but the response voltage decreases. The improvement of the bandwidth mainly comes from the increased electrical output near the maximum response voltage as shown in Figure S1b-e (Supporting Information), which is attributed to the extra oscillation generated by the load at around the resonant frequency.[33] The further increment of load weight would lead to a decrease in the bandwidth and a slight increase in the response voltage. It can be seen that the load can be employed to fine-tune the resonant frequency and improve the bandwidth without changing the size of AEH. Another merit of this parameter is that the input acoustic energy loss can be reduced by retaining the same receiving area when the AEHs with different resonant frequencies are arranged in series (Figure 1b).

2.4. Acoustoelectric Conversion and Application

The acoustoelectric sensitivity (S_a) of AEH with the resonant frequency of 200 Hz is calculated by the ratio of the open-circuit output voltage to the incident sound pressure.[34] As shown in **Figure 5**a, the maximum acoustoelectric sensitivity of AEH (PVDF diameter: 82.1 mm, the load: 0.005 g) can be calculated by:

$$\text{Sensitivity} = V/P = V/\left(P_0 \times 10^{L_p/20}\right) \quad (1)$$

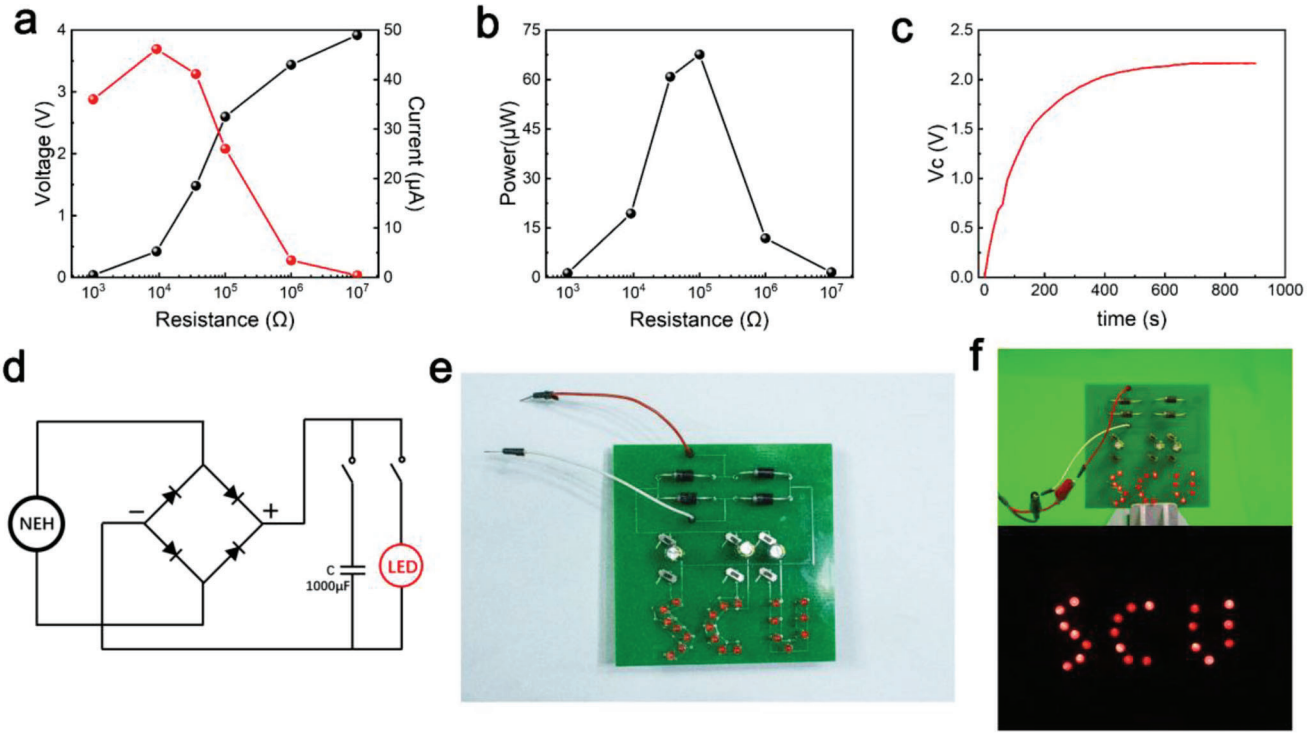

Figure 5. a) Variations of output voltage and current and b) power with external load resistance; c) Capacitor (1000 μF) charging performance of the AEH by harvesting acoustic energy from the sound wave at 200 Hz and 100 dB SPL; d) a schematic diagram of the circuit for lighting LED; e) a circuit layout for lighting the SCU logo composed of 21 LEDs. f) Photos of lighting LEDs by the AEH in the bright and dark ambient conditions, respectively (see Movie S2, Supporting Information).

where V is the output voltage under a monochromatic sound wave input, P_0 is the reference sound pressure whose value is 0.00002 Pa, and L_p is the SPL in dB. The sensitivity is 1 V Pa^{-1} at 100 dB (or 2 Pa). Furthermore, the output power of AEH at the SPL of 100 dB is quantified by measuring the piezoelectric output voltage as a function of external load resistance (R_L) from 1 kΩ to 10 MΩ. The output voltage increases gradually with the increment of R_L and gets saturated at high resistance. In contrast, the output current exhibits the opposite behavior as the load resistance increases (Figure 5a). Thus, the instantaneous maximum output power of AEH is ≈16.9 μW at an external load resistance of 0.17 MΩ (Figure 5b), which is higher than those reported PVDF-based AEH.[19] The electrical output power generated by the AEH can be calculated by:

$$P_{device} = \frac{V^2}{2R} = 8.45\mu\text{W} \tag{2}$$

To demonstrate the practical application of the device, the AEH is connected to a 1000-μF capacitor through a full wave bridge rectifier circuit to provide the charging process as shown in Figure 5c. The AEH is able to sufficiently charge up the capacitor under the SPL of 100 dB SPL and the excitation frequency of 200 Hz and attain a steady state of 2.165 V within 690 s. Based on the capacitor charging process, the average power (P_{out}) stored inside the capacitor delivered by the AEH was ≈2.39 μW. The energy conversion efficiency factor can be calculated using the following equations:[27]

$$P_{in} = \frac{AP^2}{\rho c}\cos\theta = 12.04\mu\text{W} \tag{3}$$

$$\eta = P_{out}/P_{in} \times 100\% = 19.85\% \tag{4}$$

where P_{in} is the input sound power, P is the sound pressure, and c is the sound velocity, A is the active/working area of the device, ρ is the mass density of air, and θ is the angle between the directions of the sound propagation and the normal of the active part.

Furthermore, the power generated by AEH can be used directly to light up the LEDs. To convert the AC outputs into DC, a full wave bridge rectifier is integrated into the circuit (Figure 5d,e). The Supporting Movies show the LED lighting process through the AEH and the rectification circuit. To ensure the reliability of results, the electrolytic capacitor is fully discharged and cannot light up the LED before turning on the speaker. The verification process is conducted before harvesting sound energy and can be observed in the Supporting Information Movies. With the SPL of 100 dB, the AEH works for five minutes and eight minutes to charge 1 and 3 1000-μF electrolytic capacitors (connected in parallel), respectively. Then the electrolytic capacitor can light up 1 LED (see Movie S1, Supporting Information) and the SCU logo that is composed of 21 LEDs (see Movie S2, Supporting

Information). It should be noted that the lighting is realized without involving any external storage system.

Table 1 shows the comparisons of the acoustoelectric conversion performance of the proposed AEHs and some representative ones in the literature. It can be seen that the AEH exhibits a very high response voltage (≈2 V) and output power (≈8.45 μW) among the reported work, more importantly, the performance is achieved under the low acoustic frequency and sound pressure level without employing extra sound-pressure amplification devices. The excellent performance is mainly attributed to the special device structure. Due to the small size, the corresponding area and volume power densities are high as 0.132 μW cm^{-2} and 0.066 μW cm^{-3}, respectively. Since the incident acoustic energy is in quadratic proportion to the sound pressure, the metric is used to make further performance comparison. This metric is the harvested power normalized by the square of the sound pressure and volume or area.[20] Our bioinspired AEH exhibits a high metric of 0.0168 μW Pa^{-2} cm^{-3} or 0.0333 μW Pa^{-2} cm^{-2}) that are comparable to the bulk AEHs fabricated using the multiple piezoelectric ceramics and resonator as well as the complex AEHs fabricated using piezoelectric polymer nanofiber. The promising performance of the bioinspired AEH can be realized using only a single commercial polymer membrane. Besides the very simple structure, the AEH is light with a weight of only ≈95 g that is mainly come from the copper housing. The weight can be further reduced if using a lighter material such as polymer. Overall, the bioinspired PVDF membrane exhibits excellent properties of compactness, lightweight, simple structure, and high metric.

To harvest the multi-frequency sound, the AEHs with different resonant frequencies are arranged in series as shown in Figure 1b. To keep the receiving area identical, the resonant frequencies of AEHs are adjusted mainly through the load weight rather than the membrane diameter. Here, the multi-frequency sound wave is formed by overlapping three single-frequency (216, 257, and 297 Hz) sound signals with the same SPL. To fully harvest the multi-frequency sound energy, the resonant frequencies of the three AEHs are set as the same as those of single-frequency sound signals. The schematic and photo of a multi-frequency test experiment are shown in **Figure 6**a,b, respectively. The three AEHs are placed in order along with the increasing frequency (AEH 1 (216 Hz), AEH 2 (257 Hz), and AEH 3 (297 Hz)), and physically separated with a distance of 2 cm so that the microphone can be inserted between the AEHs to measure the incident and outgoing sound signals. The distance between the first AEH (AEH 1) and sound source (I) is set as 6 cm.

Figure 6c shows the electrical signal acquired by the three AEH under the excitation of single-frequency sound waves of 216, 257, and 297 Hz (from top to bottom) with the same SPL, respectively. The three AEHs produce a very high voltage response only at their resonant frequencies, otherwise the response voltage is very low if the sound frequency is away from the resonant frequency. Since the AEH 3 is further away from the sound source, the response voltage is lower than the AEH 1 due to the energy dissipation of sound during the propagation process in the air. From the other point of view, the AEH is capable of recognizing the sound frequency. To further verify the frequency recognition capability, three different single-frequency sound waves are overlapped selectively to form three different dual-frequency incident sounds but with the same SPL. As shown in Figure 6d, before the sound waves approach the AEHs, two very narrow peaks with the same amplitude of near 100 dB are shown in the frequency spectra of incident sound measured by Microphone 1 (black line), corresponding to the frequencies of i) 216 Hz + 257 Hz, ii) 216 Hz + 297 Hz, and iii) 257 Hz + 297 Hz, respectively. When the sound waves approach the AEHs, the SPL drops (>12.5 dB) that correspond to the >86% decline in the acoustic energy. It indicates that the incident sound can pass through the AEHs with a low attenuation of SPL unless the resonant frequency of AEH is the same as the frequency of the sound wave, which shows the selective acoustic energy absorption in the AEHs. Moreover, only by comparing the response voltage of each AEH, the AEHs are capable of recognizing frequencies from the multi-frequency sound. Besides, the frequency spectrum of the signal acquired by the AEH in a non-resonant mode is very similar to that measured by the microphone, which means that the AEH can be used as the acoustic sensor when operated in the non-resonant mode. Finally, the triple-frequency sound (105 dB) is formed by mixing the three single-frequency sound waves (216, 257, and 297 Hz) to further investigate the performance of bioinspired AEH. Same phenomena are observed that the AEHs exhibit the selective strong absorption of the acoustic energy at the resonant frequency and the SPL of sound drops to a very low level (green line) after passing through the three AEHs. Figure 6e shows the electrical signal converted by the three AEHs, in which the peak-to-peak output voltages (*V*p-p) of AEH 1, AEH 2, and AEH 3 are 3.15, 1.03, and 0.74 V, respectively. According to the frequency spectra of electrical signals, the AEHs are capable of converting the sound with different frequencies into electrical power though the conversion is much more efficient at the resonant frequency.

To show the practicability, the electrical energy converted by the AEHs from the multi-frequency sound was used to light up LEDs by using full bridge rectifier circuit. In our experiment, it was found that the LED can be lit up only when the *V*p-p of AEH is higher than 1 V. Therefore, in order to obtain high voltage output, the three AEHs with different resonant frequencies (158, 186, and 210 Hz) were chosen and arranged tightly to reduce the acoustic energy dissipation in the gap. Each AEH can generate a very high *V*p-p (3.92, 3.24, and 2.28 V) under the multi-frequency sound wave (Figure S2, Supporting Information). By using this circuit to charge a 50 μF capacitor, each AEH can independently light up a commercial red LED (see Movie S3, Supporting Information). The result shows that the bioinspired AEHs could effectively harvest the energy from the multi-frequency sound. With the ability of frequency recognition, the AEH could be used as a self-powered acoustic sensor. To validate the possibility of the self-powered acoustic sensor, two AEHs with different resonant frequencies (216 and 257 Hz) are arranged in series and connected with the independent rectifier circuits and LED, respectively. Based on the on or off status of LED powered by a single-frequency sound, the frequency recognition can be conducted directly using the AEH without using an oscilloscope and FFT treatment (see Movie S4, Supporting Information). In short, the bioinspired piezoelectric type AEH can achieve multiple functions including acoustic energy harvesting, sound frequency recognition, and acoustic sensing.

Table 1. Comparison of acoustoelectric conversion performance of the proposed AEHs and reported representative AEHs (<500 Hz). (ϕ: diameter).

Materials and Structure	Device dimension	Sound Pressure level (SPL)		Sound frequency	Response Voltage	Power output	sensitivity	Area power densities Metric	Volume power densities Metric
		[dB]	[Pa]	[Hz]	[V]	[μW]	[mV Pa^{-1}]	[μW Pa^{-2} cm^{-2}]	[μW Pa^{-2} cm^{-3}]
Piezoelectric element+ resonator									
Multiple PZT Cantilever Plate+tube resonator[22]	40 mm × 50 mm × 420 mm	100	2	199	5.089	1148	2544.5	—	0.3418
Two PZT Cantilever + Helmholtz resonator[21]	176 mm × 176 mm × 120 mm	100	2	201	—	1430	—	—	0.09
PZT patch + Helmholtz resonator[35]	ϕ80 mm × 35 mm	100	2	217	0.522	27.2	261	—	0.034
		100	2	341	0.622	64.4	311	—	0.0805
Multiple PZT bimorph piezoelectric plates + Tube resonator[36]	40 mm × 50 mm × 420 mm	112	8	199	5	796	625	—	0.0148
PZT patch + Resonator[37]	ϕ40 mm × 32.4 mm	100	2	140	3.5	8.1	1750	—	0.0498
Multiple KNN cantilever bimorph plates + Tube resonator[38]	40 mm × 50 mm × 420 mm	94	1	194	3.8	2	3800	—	0.002
Piezoelectric transducer + Helmholtz resonator[39]	60 mm × 80 mm × 450 mm	110	6.3	95	4.5	115.2	2250	—	0.0013
Piezoelectric patch + Helmholtz resonator[40]	ϕ25 mm × 55 mm	100	2	332	0.23	3.49	115	—	0.002
PZT patch + Metamaterial structure [23]	ϕ154 mm × 20 mm	114	10	155	1.304	210	130.4	—	0.0001
PVDF membrane + Helmholtz resonator [41]	ϕ60 mm × 50 mm	94	1	453	0.413	0.244	413	—	0.0016
Multiple PVDF Cantilever + Tube resonator[19]	40 mm × 50 mm × 580 mm	110	6.3	146	1.48	2.2	234.9	—	5×10^{-5}
Piezoelectric polymer nanofiber									
(PVDF–Mg) nanofibers [25]	36 mm × 20 mm × 3.4 μm	120	20	130	6	8.5	150	0.0007	—
Electrospun PVDF nanofiber web [34]	120mm^2×40 μm	115	11.25	220	3.1	—	266	—	—
Electrospun PAN nanofiber web [27]	30 mm × 40 mm × 30 μm	117	14.2	230	58	210.3	—	0.0869	—
P(VDF-TrFE) nanofiber [42]	120 mm^2× 20 μm	115	11.25	210	14.5	141.3	—	0.0931	—
PVDF–ZnO acoustoelectric nanogenerator[43]	—	116	12.62	140	1.12	1.792	88.75	0.0013	—
PVDF/ TiO_2 nanofiber membrane[44]	600 mm^2 × 250 μm	90	0.63	—	8.8	108	26 000	4.0312	—
PVDF nano-micro fibers[45]	2.5 mm × 50mm × 2 mm	120	20	—	0.25	1.2×10^{-3}	12.5	—	—
PVDF nanofiber membrane[46]	280 mm^2 × 260 μm	—	—	—	1	51	—	—	—
PVDF/MAPbBr nanofiber membrane[47]	—	85	0.36	—	—	22.61	—	2.16049	—
PVDF nanofiber membrane[48]	200 mm × 300 mm × 25mm	86∼89	0.4∼0.56	—	0.1	—	250	—	—
PVDF/ZnS composite fiber membrane[49]	—	100	2	86	6	9.6	3000	0.0375	—
PVDF nanofiber membrane[50]	40 mm × 40mm	105	3.56	220	5.24	4.8	1472	0.0237	—
PVDF/silver nanoparticles composite nanofiber membrane[51]	—	100	2	—	0.0592	700	—	—	—

(*Continued*)

Table 1. (Continued).

Materials and Structure	Device dimension	Sound Pressure level (SPL)		Sound frequency	Response Voltage	Power output	sensitivity	Area power densities Metric	Volume power densities Metric
		[dB]	[Pa]	[Hz]	[V]	[μW]	[mV Pa^{-1}]	[μW Pa^{-2} cm^{-2}]	[μW Pa^{-2} cm^{-3}]
Electrospun PVDF nanofiber membrane[52]	—	—	—	4000	0.33	—	—	—	—
P(VDF-TrFE) nanofiber mesh[53]	18 mm^2 × 307 nm	95	1.12	250	0.2	—	—	—	—
PAN nanofiber membrane[54]	30 mm × 40 mm × 30 μm	95	1.12	230	2.6	—	1990	—	—
PAN nanofiber membrane[55]	30 mm × 40 mm × 30 μm	95	1.12	200	0.39	—	351.9	—	—
PVDF composites nanofibers[26]	50 mm × 20 mm × 60 μm	110	6.3	120	6	6.25	950	0.0262	—
Eardrum bioinspired PVDF membrane (this work)	ϕ90 mm × 20 mm	100	2	200	4	8.45	1000	0.0333	0.0168

3. Discussion

Multi-frequency vibration and different vibration modes coexist in a single piezoelectric element, which is closely related to the geometry of the piezoelectric element.[56,57] Different vibration modes would share the input mechanical energy, which also influences the energy distribution in the modes. To maximize the electrical output, one of the common approaches is to enhance a certain vibration mode while restraining other vibration modes or extra vibrations near the resonant frequency, which can be realized by specifically designing the geometric structure of the piezoelectric element. For example, assume using the same piezoelectric material, the bar has a higher electromechanical conversion efficiency than the circular disc because the lateral vibration mode is fully restrained in the bar geometry. The development of a trapezoidal diaphragm is an example of producing multi-frequency vibrations or different resonant modes in the desired frequency range by intelligently designing the geometric structure to achieve wide bandwidth for acoustic sensing applications.[58,59] These works demonstrate the great potential of geometry structural design on the modulation of the frequency dependence of vibration and electromechanical conversion performance in piezoelectric devices. Nevertheless, the major drawback of most reported approaches is that the actual electrical output may likely be decreased due to the trade-off relationship between the maximum electrical output and the bandwidth.

In this work, the geometry of the diaphragm can effectively modulate the response voltage, resonant frequency, and bandwidth, in which the structural parameters including the PVDF membrane diameter and the load weight are very easy to adjust in the fabrication process. The circular PVDF membrane can be easily tailored into different diameters by mechanical cutting. The assembling process of AEH is also very simple without involving any expensive equipment (see the Experimental Section). Besides, the cost of AEH is low, in which the commercial pure PVDF film is the most expensive component. Benefiting from these advantages, the bioinspired AEHs have great potential to achieve large-area implementation in some application scenarios such as highways, airports, high-speed trains, and factories.

Recently, the wireless sensor network (WSN) with thousands of sensor nodes shows promising in various areas including health monitoring, environmental monitoring, public safety and other fields.[60,61] The sensors are usually powered by batteries, so the replacement of batteries is needed to conduct from time to time. However, as the number of sensors is huge and sensors may not be easily accessible, the replacement of batteries could be time-consuming and high cost. The further increasing number and type of sensors would exacerbate the energy consumption such that the power supply of sensor nodes has become the core factor restricting the service life and running costs of WSNs. The ideal solution is to develop the self-powered sensors or micro-energy harvesters to power those sensors. The proposed bioinspired piezoelectric type AEH could offer a potential solution to achieve multi functions simultaneously including acoustic energy harvesting, sound frequency recognition, and acoustic sensing. Besides, the sound is almost everywhere especially at surveyed areas (traffic and public areas) where the sensors are usually placed. Though the energy density may be low, the supply of sound energy is abundant. Therefore, the proposed low-cost, lightweight, high-power metric, and multifunctional AEH could be an alternative solution to deal with the energy issue of the WSN.

4. Conclusion

In this work, we present the eardrum and cochlea bioinspired PVDF piezoelectric generators to harvest the multi-frequency acoustic energy at a relatively low sound pressure level. A commercial pure PVDF membrane with a circular diaphragm and the backload design was used to form an AEH with a certain resonant frequency. By controlling the diameter of PVDF membrane and the load weight, the resonant frequency can be accurately adjusted in the wide sound range of 100–500 Hz. Moreover, the AEH presents a high acoustoelectric conversion performance with power and acoustic sensitivity of 8.45 μW and 1 V Pa^{-1} at 100 dB and 200 Hz without using an extra sound-pressure amplifier or resonator. Due to its special structural design, a high metric of 0.0168 μW Pa^{-2} cm^{-3} or 0.0333 μW Pa^{-2} cm^{-2}

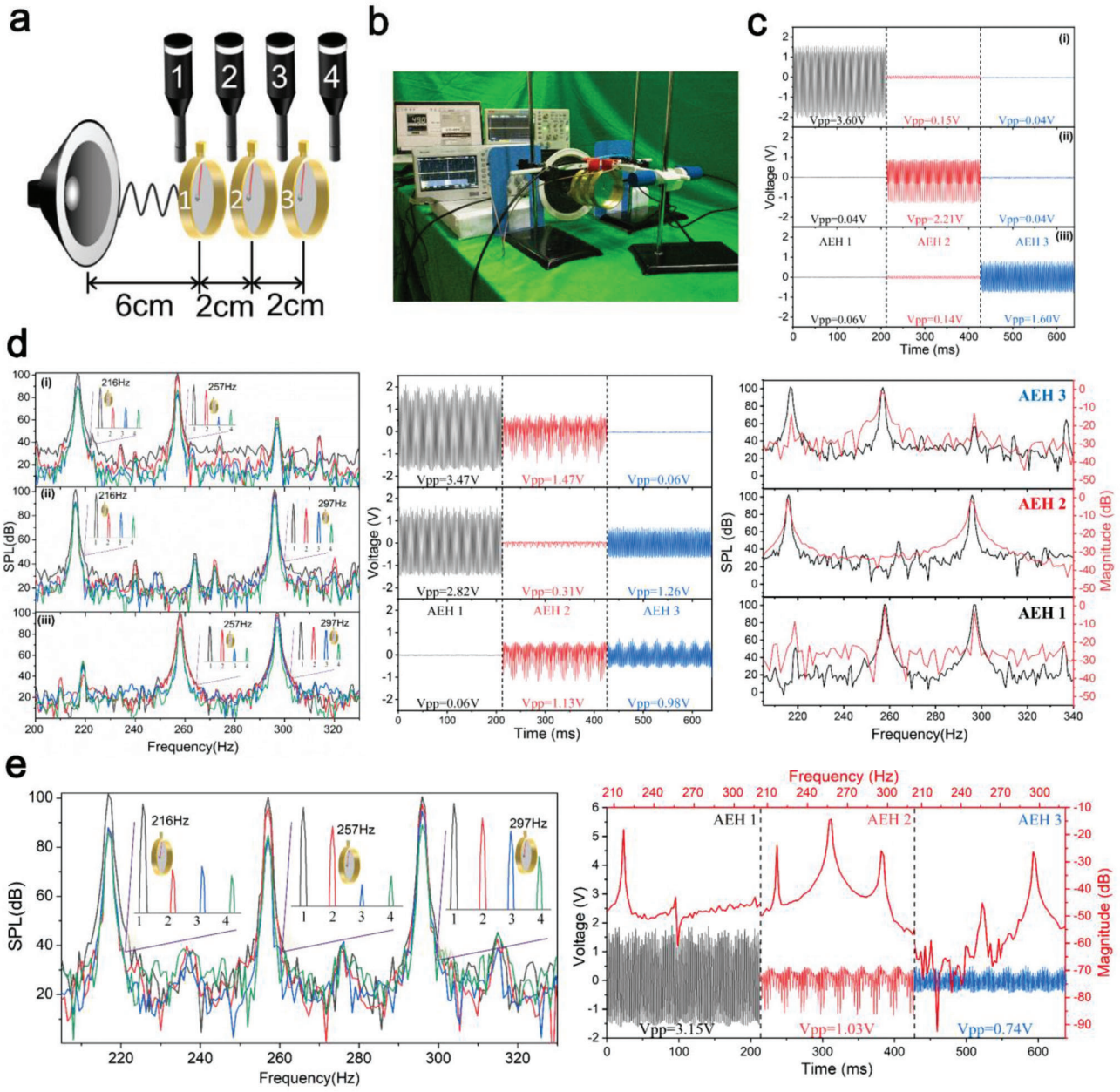

Figure 6. The a) schematic diagram and b) photo of a multi-frequency acoustic energy harvesting experimental platform; c) the electrical signal acquired by the three AEHs under the excitation of single-frequency sound (i) 216 Hz, ii) 257 Hz and iii) 297 Hz) and the SPL of 105 dB; d) the frequency spectra of the dual-frequency sound measured by four microphones, and the electrical signal acquired by the three AEHs under the excitation of dual-frequency sound (i) 216 Hz + 257 Hz, ii) 216 Hz + 297 Hz and iii) 257 Hz + 297 Hz) and the SPL of 105 dB, and the frequency spectra acquired from the AEH under the non-resonant working mode (red line) and the microphone (Black line); e) the frequency spectra of the triple-frequency sound measured by four microphones, and the electrical signal converted by the three AEHs under the excitation of the triple-frequency sound (216 Hz + 257 Hz + 297 Hz) and the SPL of 105 dB.

was measured, which is comparable to the reported AEHs fabricated using the multiple piezoelectric ceramics and resonator as well as the piezoelectric polymer nanofibers. Moreover, the bioinspired AEH cannot only harvest the acoustic energy of the multi-frequency sound to light up the LEDs, but also could recognize the sound with different frequencies even without using an oscilloscope and fast Fourier transform (FFT) processing. This low-cost, lightweight, high-power metric and multi-functional AEH could help to deal with the energy issue of the WSN.

5. Experimental Section

Fabrication of Bioinspired AEH: The bioinspired AEH was mainly composed of a copper-ring housing, an Ag-coated PVDF thick film, a back load,

conductive wires, and an SMA connector, as shown in Figure 1c. The Ag-coated PVDF thick films were composed of a 100 ± 5 µm-thick PVDF thick film and a 12 µm-thick Ag electrode layer. The piezoelectric performance of the PVDF thick film is shown in Table S1 (Supporting Information). First, the PVDF was cut into a circular shape, then fixed into a copper-ring housing and followed by filling the gap between the PVDF thick film and housing using epoxy (Epotek-301, Epoxy Technology Inc., Billerica, MA). After curing the epoxy in a dry environment for 24 h at 40 °C, a conductive Ag/polymer was subsequently cast on the surface of the epoxy gap to serve as the ground. Next, E-solder 3022 (Von Roll Isola Inc., New Haven, CT) as the back load with accurate weight was cast on the center of the back surface of the PVDF membrane. Finally, the AEH was assembled with an SMA connector and electric wires.

Electrical Output Measurements: A commercial speaker (S1-6, SAST, Ningbo, China), a power amplifier (SA-9010, SAST, Ningbo, China), and a computer were connected as the sound source, and the sound waveform and frequency were controlled by a computer software REW (Room EQ Wizard). To keep the same distance between the AEH and the loudspeaker, the AEH was fixed by a flask clamp and iron support at a distance of 10 cm from the loudspeaker. The front surface of AEH was arranged parallel to that of the loudspeaker, and these two devices were kept in line. The AEH was connected to an oscilloscope (TBS1102C, Tektronix, Beaverton, OR, USA) by a radio frequency cable (BNC male connector to SMA male connector conversion cable). The USB measurement microphone (UMM-6, Dayton Audio, Pleasant Valley, OH, USA) was placed near the surface of the AEH to monitor the frequency and SPL of the incident acoustic wave. The SPL of the incident sound was kept at 100 dB. The microphone and oscilloscope were connected to a computer to record sound signals and electrical signals. The testing platform setup is shown in Figure 3a-c.

Numerical Simulations: COMSOL Multiphysics was used for the simulation calculation. The biomimetic human-eardrum structure (a circular diaphragm with the load on the center of the back side) was generated, and then the acoustoelectric conversion performance was simulated using the multi-physics interfaces in the software: solid-mechanics interface, electrostatic interface, and acoustic-piezoelectric interaction interface. The geometric structure and structural parameters of PVDF diaphragms were designed and adjusted in the solid-mechanics interface. The built PVDF diaphragm model was meshed into the finite element using the free Tetrahedral geometry. By using the sweep frequency test method, the frequency-dependent vibration amplitude, stress distribution, resonant frequency, and response voltage of PVDF diaphragms were obtained.

Supporting Information

Supporting Information is available from the Wiley Online Library or from the author.

Acknowledgements

B.Y.D. and K.F.W. contributed to this work equally. This work was supported by the Natural Science Foundation of Sichuan Province under Grant No. 2021YJ0523.

Conflict of Interest

The authors declare no conflict of interest.

Data Availability Statement

The data that support the findings of this study are available from the corresponding author upon reasonable request.

Keywords

acoustic energy harvesters, biomimetic designs, diaphragm geometry, multi-frequency sound energy, PVDF piezoelectric generators

Received: May 27, 2023
Revised: June 17, 2023
Published online: July 2, 2023

[1] D. Briand, E. Yeatman, S. Roundy, O. Brand, G. K. Fedder, C. Hierold, J. G. Korvink, O. Tabata, *Micro Energy Harvesting*, Wiley, New York **2015**.
[2] Z. Ren, Z. Wang, Z. Liu, L. Wang, H. Guo, L. Li, S. Li, X. Chen, W. Tang, Z. L. Wang, *Adv. Energy Mater.* **2020**, *10*, 2001770.
[3] S. Madruga, *Renew. Energ.* **2021**, *168*, 424.
[4] A. Hamdan, F. Mustapha, K. A. Ahmad, A. S. M. Rafie, *Renew. Sust. Energ. Rev.* **2014**, *35*, 23.
[5] C. H. Wang, S. Wang, Z. W. Gao, Z. Song, *Appl. Energ.* **2021**, *287*, 116581.
[6] J. Choi, I. Jung, C. Y. Kang, *Nano Energy* **2019**, *56*, 169.
[7] K. J. Ma, T. Tan, Z. M. Yan, F. R. Liu, W. H. Liao, W. M. Zhang, *Nano Energy* **2021**, *82*, 105693.
[8] H. M. E. Miedema, *J. Soc. Issues* **2007**, *63*, 41.
[9] L. Gammaitoni, *Contemp. Phys.* **2012**, *53*, 119.
[10] X. Lu, D. Niyato, P. Wang, D. I. Kim, Z. Han, *Ieee Wirel. Commun.* **2015**, *22*, 126.
[11] N. M. Monroe, J. H. Lang, *Smart Mater. Struct.* **2019**, *28*, 055032.
[12] G. S. Liu, Y. Y. Peng, M. H. Liu, X. Y. Zou, J. C. Cheng, *Appl. Phys. Lett.* **2018**, *113*, 153503.
[13] J. Liu, N. Cui, L. Gu, X. Chen, S. Bai, Y. Zheng, C. Hu, Y. Qin, *Nanoscale* **2016**, *8*, 4938.
[14] S. Kulkarni, E. Koukharenko, R. Torah, J. Tudor, S. Beeby, T. O'Donnell, S. Roy, *Sensor Actuat. a-Phys.* **2008**, *145*, 336.
[15] H. M. Chen, C. Xing, Y. L. Li, J. Wang, Y. Xu, *Sustain. Energ. Fuels.* **2020**, *4*, 1063.
[16] K. Dong, X. Peng, Z. L. Wang, *Adv. Mater.* **2020**, *32*, 1902549.
[17] X. W. Mo, H. Zhou, W. B. Li, Z. S. Xu, J. J. Duan, L. Huang, B. Hu, J. Zhou, *Nano Energy* **2019**, *65*, 104033.
[18] G. M'boungui, K. Adendorff, R. Naidoo, A. A. Jimoh, D. E. Okojie, *Renew. Sust. Energ. Rev.* **2015**, *49*, 1136.
[19] B. Li, A. J. Laviage, J. H. You, Y.-J. Kim, *Appl. Acoust.* **2013**, *74*, 1271.
[20] M. Yuan, Z. Cao, J. Luo, X. Chou, *Micromachines-Basel* **2019**, *10*, 48.
[21] A. Yang, P. Li, Y. Wen, C. Lu, X. Peng, W. He, J. Zhang, D. Wang, F. Yang, *Rev. Sci. Instrum.* **2014**, *85*, 066103.
[22] B. Li, J. H. You, Y. J. Kim, *Smart Mater. Struct.* **2013**, *22*, 055013.
[23] M. Yuan, Z. P. Cao, J. Luo, R. Ohayon, *J. Low. Freq. Noise V. A.* **2018**, *37*, 1015.
[24] K. S. Ramadan, D. Sameoto, S. Evoy, *Smart Mater. Struct.* **2014**, *23*, 033001.
[25] B. Mahanty, S. K. Ghosh, S. Jana, K. Roy, S. Sarkar, D. Mandal, *Sustain. Energ. Fuels.* **2021**, *5*, 1003.
[26] K. Roy, S. Jana, Z. Mallick, S. K. Ghosh, B. Dutta, S. Sarkar, C. Sinha, D. Mandal, *Langmuir* **2021**, *37*, 7107.
[27] H. Shao, H. X. Wang, Y. Y. Cao, X. Ding, J. Fang, H. T. Niu, W. Y. Wang, C. H. Lang, T. Lin, *Nano Energy* **2020**, *75*, 104956.
[28] X. M. Cai, T. P. Lei, D. H. Sun, L. W. Lin, *RSC Adv.* **2017**, *7*, 15382.
[29] S. S. Panicker, S. P. Rajeev, V. Thomas, *Nano-Structures&Nano-Objects* **2023**, *34*, 100949.
[30] M. Khaleghi, C. Furlong, J. T. Cheng, J. J. Rosowski, presented at Mechanics of Biological Systems and Materials, 6: Proceedings of the 2015 Annual Conference on Experimental and Applied Mechanics **2016**.
[31] R. U. Ahmed, S. Banerjee, presented at *Bioinspiration, Biomimetics, and Bioreplication 2016*, Las Vegas, Nevada, United States **2016**.
[32] H. Güleç, M. Gurbuz, A. G. Toktas, M. Gul, B. Koc, A. Dogan, *Journal of the Australian Ceramic Society* **2020**, *56*, 117.
[33] S. J. Zhu, Y. F. Zheng, Y. M. Fu, *J. Sound Vib.* **2004**, *271*, 15.

[34] C. Lang, J. Fang, H. Shao, X. Ding, T. Lin, *Nat. Commun.* **2016**, *7*, 11108.
[35] M. Yuan, Z. P. Cao, J. Luo, Z. Q. Pang, *Aip. Adv.* **2018**, *8*, 085012.
[36] B. Li, J. H. You, *J. Intel. Mat. Syst. Str.* **2015**, *26*, 1646.
[37] M. Yuan, X. Sheng, Z. P. Cao, Z. Q. Pang, G. L. Huang, *Smart Mater. Struct.* **2020**, *29*, 035012.
[38] A. Kumar, A. Sharma, R. Kumar, R. Vaish, C. R. Bowen, *Ferroelectrics* **2016**, *504*, 149.
[39] C. Gu, Y. S. Chen, K. Jiang, *Aip. Adv.* **2021**, *11*, 025031.
[40] M. Yuan, Z. P. Cao, J. Luo, J. Y. Zhang, C. Chang, *Sensor Actuat. a-Phys.* **2017**, *264*, 84.
[41] X. D. Zhang, H. L. Zhang, Z. S. Chen, G. Wang, *Smart Mater. Struct.* **2018**, *27*, 105018.
[42] C. H. Lang, J. Fang, H. Shao, H. X. Wang, G. L. Yan, X. Ding, T. Lin, *Nano Energy* **2017**, *35*, 146.
[43] B. L. Sun, X. Li, R. Zhao, H. Ji, J. Qiu, N. Zhang, D. Y. He, C. Wang, *J. Mater. Sci.* **2019**, *54*, 2754.
[44] M. M. Alam, A. Sultana, D. Mandal, *Acs Appl. Energ. Mater.* **2018**, *1*, 3103.
[45] T. H. Lee, C. Y. Chen, C. Y. Tsai, Y. K. Fuh, *Polymers-Basel* **2018**, *10*, 692.
[46] K. Maity, D. Mandal, *ACS Appl. Mater. Interfaces* **2018**, *10*, 18257.
[47] A. Sultana, M. M. Alam, P. Sadhukhan, U. K. Ghorai, S. Das, T. R. Middya, D. Mandal, *Nano Energy* **2018**, *49*, 380.
[48] E. Ghafari, N. Lu, *Compos. Part B-Eng.* **2019**, *160*, 1.
[49] A. Sultana, M. M. Alam, S. K. Ghosh, T. R. Middya, D. Mandal, *Energy* **2019**, *166*, 963.
[50] Y. J. Hwang, S. Choi, H. S. Kim, *Sensor Actuat. a-Phys* **2019**, *300*, 111672.
[51] C. M. Wu, M. H. Chou, *eXPRESS Polym. Lett.* **2020**, *14*, 103.
[52] N. Shehata, A. H. Hassanin, E. Elnabawy, R. Nair, S. A. Bhat, I. Kandas, *Sensors-Basel* **2020**, *20*, 3111.
[53] W. Y. Wang, P. N. Stipp, K. Ouaras, S. Fathi, Y. Y. S. Huang, *Small* **2020**, *16*, 2000581.
[54] H. Shao, H. X. Wang, Y. Y. Cao, X. Ding, J. Fang, W. Y. Wang, X. Jin, L. Peng, D. Q. Zhang, T. Lin, *Adv. Electron. Mater.* **2021**, *7*, 2100206.
[55] L. Peng, X. Jin, J. R. Niu, W. Y. Wang, H. X. Wang, H. Shao, C. H. Lang, T. Lin, *J. Mater. Chem. C* **2021**, *9*, 3477.
[56] S. Dhote, H. T. Li, Z. B. Yang, *Int. J. Mech. Sci.* **2019**, *157*, 684.
[57] M. Rezaeisaray, M. El Gowini, D. Sameoto, D. Raboud, W. Moussa, *Sensor Actuat. a-Phys* **2015**, *228*, 104.
[58] J. H. Han, J. H. Kwak, D. J. Joe, S. K. Hong, H. S. Wang, J. H. Park, S. Hur, K. J. Lee, *Nano Energy* **2018**, *53*, 198.
[59] H. Shintaku, T. Nakagawa, D. Kitagawa, H. Tanujaya, S. Kawano, J. Ito, *Sensor Actuat. a-Phys.* **2010**, *158*, 183.
[60] F. Wen, H. Wang, T. Y. Y. He, Q. F. Shi, Z. D. Sun, M. L. Zhu, Z. X. Zhang, Z. G. Cao, Y. B. Dai, T. Zhang, C. K. Lee, *Nano Energy* **2020**, *67*, 104266.
[61] W. Saad, M. Bennis, M. Chen, *IEEE network* **2019**, *34*, 134.